Progress of Theoretical Physics, Vol. 111, No. 4, April 2004

Properties of Kaluza-Klein Black Holes

Hideaki KUDOH[1,*)] and Toby WISEMAN[2,**)]

[1] *Department of Physics, Kyoto University, Kyoto 606-8502, Japan*
[2] *Jefferson Physical Laboratory, Harvard University, Cambridge, MA 02138, USA*

(Received November 9, 2003)

We detail numerical methods to compute the geometry of static vacuum black holes in 6-dimensional gravity compactified on a circle. We calculate properties of these Kaluza-Klein black holes for varying mass, keeping the asymptotic compactification radius fixed. For increasing mass, the horizon deforms into a prolate ellipsoid, and the geometry near the horizon and axis decompactifies. We are able to find solutions with horizon radii approximately equal to the asymptotic compactification radius. Having chosen 6 dimensions, we may compare these solutions to those of non-uniform strings compactified on a circle of the same radius found in a previous numerical work. We find the black holes achieve larger masses and horizon volumes than most non-uniform strings. This sheds doubt on whether these solution branches can merge via a topology changing solution. Further work is required to resolve whether there is a maximum mass for the black holes, or whether the mass can become arbitrarily large.

§1. Introduction

If one day we discover that there are extra dimensions in our universe, and these are well described by classical gravity, then they are likely (although not definitely[1)]) to be compact along the lines of Kaluza-Klein theory.[2),3)] Furthermore, if matter is confined to branes, then the radius of compactification could potentially be extremely large.[4),5)] The simplest regular static vacuum solutions are then compactified uniform black strings.[6),7)] Gregory and Laflamme (GL) showed that these are stable, provided that the horizon radius is large compared to the compactification scale.[8)–10)] However, they also discovered a new family of non-uniform solutions emerging from the critical uniform string whose mass separates the more massive stable strings from the less massive unstable ones. These non-uniform solutions were constructed numerically, first by Gubser as a perturbation expansion in a non-uniformity parameter λ about the $\lambda = 0$ critical uniform solution,[11)] and then non-perturbatively in Ref. 12) using elliptic methods. The third class of solutions expected to exist are black holes that do not wrap in the circle direction. In 4 dimensions, such solutions were found by Myers analytically[13)] (see also generalisations given in Refs. 14) and 15) with modified asymptotics) but in greater than 4 dimensions little is known,[16),17)] essentially as the rotation group then has curvature. Using the elliptic numerical methods of Refs. 12) and 18), 5 dimensional localised black holes have recently been constructed on a Randall-Sundrum brane.[19),20)] This is a related numerical problem of considerable interest, as recent conjectures claim

*) E-mail: kudoh@yukawa.kyoto-u.ac.jp
**) E-mail: twiseman@fas.harvard.edu

that large localised static black holes may not exist.[21),22)]

Kol proposed an elegant relation between these three types of Kaluza-Klein solutions,[23)] the non-uniform strings linking the uniform branch to the black hole branch. The string to the black hole transition, also explored in Refs. 17), 24)–28), is then conjectured to be continuous and have a Lorentzian cone geometry where the horizon becomes degenerate. This agrees very well with numerical tests on the non-uniform string branch.[29),30)] If this picture is correct, it predicts that black holes, like non-uniform strings, have a maximum mass. While for a fixed compactification radius, the three classes of solutions overlap at intermediate mass scales,[*)] at large masses the uniform strings would be the unique non-singular solutions in Kaluza-Klein theory. If this picture is incorrect, it may be possible to have arbitrarily large mass black holes, if either the geometry becomes increasingly 'squashed' or decompactifies on the symmetry axis (as in pure Kaluza-Klein theory there is no radius stabilisation). Whether this could persist in a radius stabilised theory would then be an important phenomenological question.

Clearly Kaluza-Klein theory is a simplification of realistic compactifications. Kol's picture presumably remains unchanged when warping is added,[33)–36)] or when black holes are charged under matter fields localised to branes.[37)] For additional bulk matter, such as is necessary for stabilisation, the situation may be more interesting, but we expect that it will inherit many features of the pure Kaluza-Klein case.

The Gregory-Laflamme instability, underlying the dynamics of these compactified horizons, has been linked to thermodynamic stability,[36),38)–45)] and an analogous classical instability has recently been conjectured for the rotating Myers-Perry solution,[46)–48)] which is thought to be unstable for large angular momenta. The end state of the classical Gregory-Laflamme instability is still a mystery, although there has been interesting analytic and numerical work on this subject.[49),50)] We note that stable black strings evaporating via Hawking radiation will eventually succumb to this classical instability, and understanding the dynamics, and in particular whether cosmic censorship is violated, is important in order to understand the evaporation of cosmological/astrophysical black holes below the compactification mass scale.

The objective of this paper is to numerically construct and study the non-wrapping black hole branch of solutions. We perform this analysis in 6 dimensions so that we can compare our results with the previous non-uniform string numerical results of Ref. 12), which for technical reasons, were performed in this number of dimensions. We begin with a brief discussion of the numerical method, which involves phrasing a subset of the Einstein equations in a way compatible with numerical relaxation, and most importantly, showing how the remaining 'constraint' equations can be satisfied by appropriately choosing the boundary conditions. Since the method has been used several times,[12),18),19)] we refrain from a detailed exposition, and instead highlight the various subtleties related to this Kaluza-Klein black hole problem. We then go on to discuss the numerical results. We demonstrate

[*)] We must consider the full asymptotic charges to distinguish the solution,[26),27)] although whether there is a unique solution with these charges is an interesting open question,[28)] as uniqueness constraints apparently weaken in greater than 4 dimensions.[31),32)]

that, as expected, these solutions do exist, at least within the scope of our numerical approximation.

We compute geometric embeddings of the spatial horizon and symmetry axis into Euclidean space, and show that the geometry near the axis decompactifies with increasing mass, and the event horizon deforms into a prolate ellipsoid. With the current implementation we are unable to ascertain whether this decompactification terminates with a maximum mass black hole that just 'fits' into the compact direction, or whether the decompactification continues indefinitely, so that arbitrarily large masses can be found.

The maximum size black holes that we are able to construct have horizon radii approximately equal to the asymptotic compactification radius. We compare these with the most non-uniform strings constructed in Ref. 12) finding the mass and horizon volume of these modest-sized black holes already are larger than those of the maximally non-uniform strings, and the axis decompactifies to a greater extent. The size of the black holes we can construct is limited by numerical factors, and it seems clear that still larger black holes exist, with the above trends continuing for these. The implication is that it appears *unlikely* that the non-uniform string branch (connected to the critical uniform string) and *this* black hole branch are connected via a topology changing solution.

Various technical details and numerical checks are given in the three appendices. We pay particular attention to ensuring and checking that the constraint equations are indeed satisfied for the solutions.

The reader is also referred to an independent work by Kol, Piran and Sorkin, who, we understand, have recently performed related calculations in 5 dimensions.[51)]

§2. Method

In order to solve the black hole geometry we are required to solve the Einstein equations with elliptic boundary data; we wish to have a regular horizon geometry, for the solution to be periodic, and also asymptotically to tend to a flat space product with a circle. We employ the methods first developed in Ref. 18) and used to construct non-uniform string solutions,[12)] and later localised black holes on branes.[19),20),*)] In this section, we outline the method and boundary conditions appropriate for the problem. Due to its necessarily technical nature, some readers may wish to skip to the following 'Results' section. For a more general discussion of the method, the reader is referred to Ref. 12). Technical numerical details are also provided for the interested reader in Appendix A, and important numerical checks are reported in Appendix B to demonstrate that the method functions correctly.

The construction of non-uniform strings is a very clean situation in which to apply these elliptic numerical methods. However, the black hole problem at hand is substantially more difficult, primarily for two reasons.

Firstly, weakly non-uniform strings can be described as perturbative deforma-

*) See also Ref. 52) for a method of solving static axisymmetric *non-vacuum* black holes in 4 dimensions that shares some features with our method.

tions of the critical uniform string. The relaxation methods employed here require a good initial guess, or typically no solution will be found. Thus for the strings, the non-uniformity can be turned on 'gently'. In analogy, a very small black hole will appear as a 6-d Schwarzschild solution near its horizon, but it obviously must have very different asymptotics, due to the compactification. Thus, even for a small black hole, we do not have an exact solution from which to 'gently' start building larger black holes. We tackle this issue by building in 6-d Schwarzschild behaviour at the horizon that decays quickly away far from the horizon, and then we solve for the correction to this, which should be small for small mass black holes.

Secondly, the axis of symmetry is exposed in the problem. The coordinate singularity at the axis generically gives rise to problems in numerical computations and there are various ways around this in conventional evolution problems (see for example Ref. 53)). As discussed in Ref. 18) the elliptic method we use is very sensitive to this coordinate singularity, which may destroy the ability of the algorithm to relax to the solution. Furthermore the coordinate system we require to phrase a subset of the Einstein equations in an elliptic manner introduces even worse coordinate problems on the symmetry axis than one would normally expect. We have found no elegant method to tackle this problem, but we do have a functional approach, originally used in Ref. 18) and discussed here in Appendix A. Improving or evading this problem appears to be crucial for increasing the capability of this method.

So whilst the problem is a rather delicate one, we are still able to make progress. As in previous applications of the method, we write the static axisymmetric metric in a diagonal form, retaining conformal invariance in the radial and tangential coordinates r and z as

$$ds^2 = g_{MN}dx^M dx^N = -e^{2\alpha}dt^2 + e^{2(\beta-\gamma)}\left(dr^2 + dz^2\right) + r^2 e^{2\beta+\frac{4}{3}\gamma}d\Omega^2_{(3)} \qquad (1)$$

with α, β and γ being functions of r and z. The particular linear combination of β and γ taken above is simply for later technical convenience. We take the z coordinate to be compact with period L, and later we require the metric functions α, β and γ to vanish for large r, and hence the physical radius of compactification becomes L. We choose units such that the 6-dimensional Newton constant is unity: $G_{N(6)} = 1$. Since we may perform a global scaling on any solution of the vacuum Einstein equations, for future convenience we choose to set $L = \pi$ in these units.

One nice property of this form of the metric is that one can choose the position of the boundaries in the (r, z) plane to be at any location, due to the residual conformal coordinate transformations. A second important feature of this coordinate system is that 3 of the 5 Einstein equations, $G^t{}_t, (G^\rho{}_\rho + G^\chi{}_\chi)$ and $G^\theta{}_\theta$ have elliptic second derivatives, being just the (r, z) Laplace operators, and thus we term these the 'elliptic' equations. As we are so far unable to write a positive definite functional of the metric components that can be minimized to give these equations, it is not at all clear if the problem is truly elliptic. However one can still use relaxation methods to solve them, specifying elliptic data on the boundaries of the problem. The most important feature of this coordinate system is that using the contracted Bianchi

identities, the 2 remaining 'constraint' equations weighted by $\det g_{MN}$,

$$\hat{\Phi} = \det g_{MN} G^r{}_z, \qquad \hat{\Psi} = \frac{1}{2} \det g_{MN} (G^r{}_r - G^z{}_z), \tag{2}$$

obey the Cauchy-Riemann (CR) relations,

$$\partial_r \hat{\Phi} = \partial_z \hat{\Psi}, \qquad \partial_z \hat{\Phi} = -\partial_r \hat{\Psi}, \tag{3}$$

if the elliptic equations are satisfied. Simply relaxing the 3 elliptic equations for the 3 metric functions will generically yield a solution, but this is *only* consistent with the full set of Einstein equations if the boundary data are such that the CR relations imply both constraints are satisfied. For example, for the non-uniform strings, we may impose the constraints by updating the elliptic boundary data such that the $G^r{}_z$ constraint is satisfied on all boundaries, and the remaining constraint $(G^r{}_r - G^z{}_z)$ is just imposed at one point, solving the CR problem.[12] In our example here, we in fact find it convenient to impose both constraints, but on different boundaries, in such a way that still provides sufficient conditions to satisfy the CR problem, but does not over determine the elliptic equations.

2.1. *Boundaries and coordinates*

We still have residual coordinate freedom, and we use this to tailor the coordinate system to our problem. Instead of relaxing α, β and γ directly, we wish to perturb about a 6-d Schwarzschild solution near the horizon,

$$\alpha = A_{bg} + A, \qquad \beta = B_{bg} + B, \qquad \gamma = C_{bg} + C, \tag{4}$$

where the 'background functions' $\{A, B, C\}_{bg}$ suitably express this Schwarzschild geometry at the horizon, decay away radially, and are compatible with the compact boundary conditions; therefore we could obviously not just take the Schwarzschild metric itself. Notice that $C = 0$ corresponds to conformally flat spatial sections.

Let us now consider a form for the background functions and the boundary locations in the (r, z) coordinates. The 6-d Schwarzschild metric can easily be written in an appropriate conformal form as

$$\begin{aligned} ds^2 &= -n(\mu) dt^2 + a(\mu) \left(d\mu^2 + \mu^2 d\Omega^2_{(4)} \right), \\ &= -\left[\frac{\mu^3 - \mu_0^3}{\mu^3 + \mu_0^3} \right]^2 dt^2 + \left[1 + \frac{\mu_0^3}{\mu^3} \right]^{\frac{4}{3}} \left(dr^2 + dz^2 + r^2 d\Omega^2_{(3)} \right), \end{aligned} \tag{5}$$

with $\mu^2 = r^2 + z^2$. To be suitable for the background functions, this must be modified away from the horizon to ensure compatibility with the periodic boundary conditions in z. However, assuming after this modification that the horizon remains at constant $\mu = \mu_0$, it will form a circle in the (r, z) coordinates. Thus, we would wish to use boundaries of the form in Fig. 1 in order to represent the coordinate axis, the black hole horizon, and periodic boundaries. Then we would reasonably expect the functions A, B and C to remain finite everywhere and be small for a small black hole, allowing us to use the initial data $A = B = C = 0$ for the relaxation.

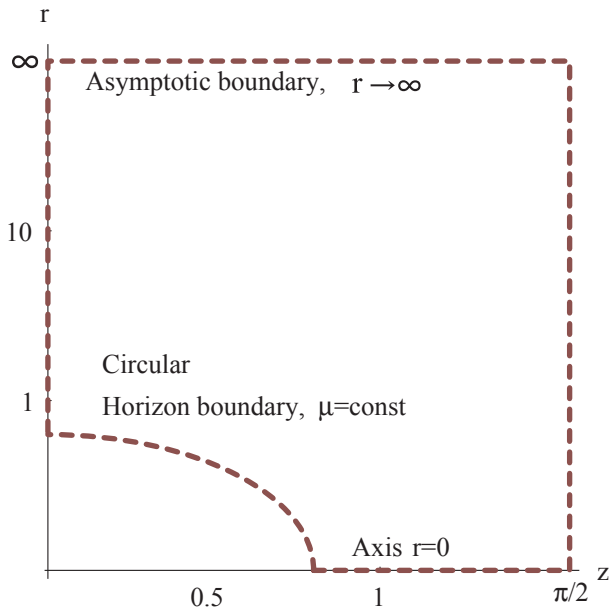

Fig. 1. Schematic illustration of the boundaries we would intuitively take in r and z coordinates. At least for small black holes, taking the horizon boundary to be circular would ensure the metric functions A, B and C be small and finite, as the geometry near the horizon would be only a weak distortion of the 6-dimensional Schwarzschild geometry, which we build into the metric ansatz via A_{bg}, B_{bg} and C_{bg}.

Numerically, it is always convenient to have a rectangular grid. Whilst we are in principle free to use the residual conformal transformation to fix the boundaries to be wherever we wish, clearly to obtain a rectangular domain such a transformation must be singular, as one right angle in Fig. 1 should be 'flattened' out. However, if we find such a coordinate transformation analytically, we may separate out any singular behaviour from A, B and C, leaving their behaviour perfectly regular. Any conformal coordinate transformation is generated by a solution to the 2-d Laplace equation, and choosing a solution $\rho(r, z)$ to be that representing a point source in the compact 2-d space (i.e. on a cylinder) we define the new coordinates (ρ, χ)

$$\rho(r, z) = \frac{1}{2} \log \left[\frac{1}{2} \left(\cosh 2\, r - \cos 2\, z \right) \right],$$
$$\chi(r, z) = \tan^{-1} \left[\frac{\tan z}{\tanh r} \right], \tag{6}$$

where χ is determined from ρ by CR relations. These essentially 'flatten' out the horizon, and now χ is the compact coordinate which conveniently takes the range of an angular coordinate $(0, \pi/2)$ for half a period of the solution, $z = (0, L/2) = (0, \pi/2)$. We illustrate the isosurfaces of ρ and χ in the (r, z) plane in Fig. 2. Contours of constant ρ, for $\rho < 0$, generate curves in the (r, z) plane that are very similar to that of the horizon in Fig. 1. Note also that $\chi = \pi/2$ gives *both* the axis of symmetry (for $\rho < 0$) *and* the periodic boundary $z = \pi/2$ (for $\rho > 0$), and $\rho = 0$, $\chi = \pi/2$ is the

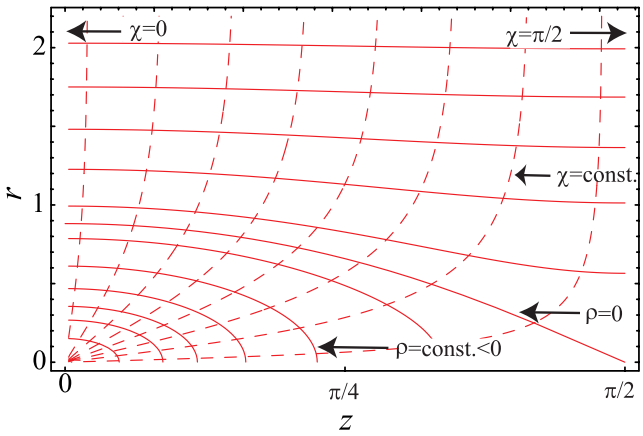

Fig. 2. Illustration of isosurfaces of ρ and χ as functions of r, z. The schematic boundaries of Fig. 1 can be mapped to constant ρ and χ values, allowing for convenient numerical implementation. For $\rho < 0$, χ behaves as an angular coordinate, and ρ as a radial one, whereas for large positive ρ, we find that ρ and χ behave as r and z, respectively. We take the horizon boundary at constant $\rho = \rho_0$, finding later that specifying ρ_0 determines the physical size of the black hole solution.

singular point in the conformal transformation. Thus if we use these coordinates, a rectangle with $\chi = 0$ to $\pi/2$ and $\rho = \rho_0$ to ∞ will, for $\rho_0 < 0$, give boundaries that are similar to those in Fig. 1.

Whilst the coordinate transform is rather singular, since we have an analytic expression for it, we may remove the singular Jacobian, J, and then write the metric as

$$ds^2 = -e^{2\alpha}dt^2 + e^{2(\beta-\gamma)}J(\rho,\chi)\left(d\rho^2 + d\chi^2\right) + r(\rho,\chi)^2 e^{2\beta+\frac{4}{3}\gamma}d\Omega^2_{(3)}, \tag{7}$$

$$J(\rho,\chi) = \frac{e^{2\rho}}{\sqrt{1+e^{4\rho}+2\,e^{2\rho}\cos 2\chi}},$$
$$r(\rho,\chi) = \frac{1}{2}\cosh^{-1}\left[e^{2\rho} + \sqrt{1+e^{4\rho}+2\,e^{2\rho}\cos 2\chi}\right],$$

where now α, β and γ are exactly the same functions as in (1), except now expressed in terms of ρ and χ.

Now consider the 6-d Schwarzschild metric (5). For small μ_0, near the horizon we find $e^{2\rho} \simeq \mu^2 = r^2 + z^2$, with ρ behaving as a polar radial coordinate and χ as an angular one. Since we wish to choose background functions to reproduce the Schwarzschild metric near the horizon for small black holes (i.e. small μ_0), and yet to implement the compactness requirement in z, a simple choice is just to substitute $e^{\rho-\rho_0} = \mu/\mu_0$ into (5), giving

$$e^{A_{bg}} = \frac{1-e^{3(\rho_0-\rho)}}{1+e^{3(\rho_0-\rho)}},$$
$$e^{B_{bg}} = \left[1+e^{3(\rho_0-\rho)}\right]^{\frac{2}{3}},$$

$$C_{bg} = 0. \tag{8}$$

The independence of these background functions on χ ensures that they satisfy the periodicity requirements. The constant ρ_0 tells us the coordinate position of the horizon. We will shortly show that keeping the asymptotic compactification radius fixed, it is the parameter ρ_0 (and thus the contour $\rho = \rho_0$ we take to be the horizon) that we vary to change the mass of the black hole. From Fig. 2 we see that ρ_0 must be negative to give a spherical topology for the horizon. The small horizon limit is now $\rho_0 \to -\infty$. For $\rho_0 < 0$ but closer to zero, the ansatz above gives a deformed geometry from the Schwarzschild geometry too.*) Since we include the vanishing of the lapse in A_{bg} at $\rho = \rho_0$, we expect the metric functions, and in particular A, the one associated with deformations of the lapse, to remain finite there. Far away from the horizon, i.e. for $\rho \to \infty$, or alternatively $r \to \infty$, the background functions decay exponentially in ρ or r. We stress that for finite negative ρ_0, $A, B, C = 0$ is *not* a solution to the Einstein equations, but for very large negative values of ρ (i.e. the small black hole limit), A, B and C will at least be small everywhere as the horizon tends to the Schwarzschild geometry, and by the time the metric functions 'see' the compactification they will be varnishingly close to zero anyway. After the change in coordinates, we obtain analogous elliptic equations, $G^t{}_t, (G^\rho{}_\rho + G^\chi{}_\chi)$ and $G^\theta{}_\theta$ and also CR relations for the new constraint functions Φ and Ψ:

$$\Phi = \det g_{MN} G^\rho{}_\chi, \qquad \Psi = \frac{1}{2} \det g_{MN} (G^\rho{}_\rho - G^\chi{}_\chi) \tag{9}$$

so that,

$$\partial_\rho \Phi = \partial_\chi \Psi, \qquad \partial_\chi \Phi = -\partial_\rho \Psi. \tag{10}$$

2.2. *Boundary conditions from the elliptic equations*

The 3 elliptic equations we are solving require various boundary conditions due to the regular singular or periodic behaviour at these boundaries. To satisfy the constraint equations we must impose more than just these conditions. However, let us start by considering the basic boundary conditions from the elliptic equations.

Asymptotically we want the geometry to be a product of 5-dimensional flat space with a circle, and thus we take $A, B, C \to 0$. Since we earlier fixed the range of χ, this also fixes the compactification radius to be $L = \pi$. Of course we may simply globally scale these vacuum solutions to obtain any desired asymptotic radius. We

*) It is interesting to compare this coordinate system with that proposed by Harmark and Obers in Ref. 17) where the radial coordinate used follows a 6-d equipotential. Here, our coordinate follows a 2-d equipotential. Presumably, using the higher-dimensional potential is a sensible procedure, and it could give an improved ansatz to perturb about, which better models the horizon geometry for larger deformed black holes. It is an interesting problem to use the ansatz of Harmark and Obers to do numerics, particularly as the ansatz and having the horizon at a location with constant potential were proven to be consistent for non-uniform strings in Ref. 29) and recently for black holes in Ref. 28).

find the asymptotic forms required by the 3 elliptic equations,

$$A \sim \frac{a_2}{\rho^2} + O\left(\frac{1}{\rho^3}\right), \quad B \sim \frac{b_1}{\rho} + \frac{b_2}{\rho^2} + O\left(\frac{1}{\rho^3}\right), \quad C \sim \frac{b_1}{\rho} + \frac{c_2}{\rho^2} + O\left(\frac{1}{\rho^3}\right), \quad (11)$$

$$\text{with} \qquad 3\,a_2 + 9\,b_2 - 4\,c_2 + \frac{25}{6} b_1^2 = 0$$

by expanding (without linearising in the metric components) in inverse powers of $\rho \sim r$. Fourier modes with χ dependence decay exponentially (since $\chi \simeq z$, for large ρ), as does the contribution from the background functions $\{A, B, C\}_{bg}$. Thus on our asymptotic boundary we have mixed Neumann-Dirichlet boundary conditions for the 3 metric functions.*)

The symmetry axis $\chi = \pi/2$ with $\rho < 0$ requires that A and B be even in $(\chi - \pi/2)$ (or alternatively r). However we also find the requirement $C = 0$, as there is regular singular behaviour due to the form of the coordinate system. We might be confused that there is no Neumann condition on C but we see later that this emerges from the constraints.

We require that the metric functions A, B and C be finite at the horizon $\rho = \rho_0$. With the form of background functions $\{A, B, C\}_{bg}$, we then find that the elliptic equations are consistent, provided that

$$\begin{aligned} A_{,\rho} \mid_{\rho=\rho_0} &= 0, \\ B_{,\rho} + \frac{2}{3} C_{,\rho} \mid_{\rho=\rho_0} &= 1 - \frac{r_{,\rho}}{r} \mid_{\rho=\rho_0}, \end{aligned} \quad (12)$$

with $r(\rho, \chi)$ as given in Eq. (7).

Finally, the elliptic equations at the remaining periodic boundaries at $\chi = 0$ and $\chi = \pi/2$ with $\rho > 0$ simply imply Neumann conditions on the metric functions A, B and C.

2.3. *Boundary conditions from the constraints*

The constraint equations also impose conditions on the metric. We have seen that assuming we can satisfy the elliptic equations for given boundary data, the two constraints obey the CR relations. Thus we do not need to enforce both constraints on all the boundaries, which naively would over-determine the elliptic equations. Firstly we consider the extra conditions that the constraints impose, and then discuss how best to implement them to ensure a consistent solution of the CR problem, without over determining the elliptic data.

On the symmetry axis and periodic boundaries, we have already specified 3 conditions, one for each metric function, and consequently treating this as a boundary value problem, we do not wish to impose any more. On the $\chi = 0$ periodic boundary, $G^{\rho}{}_{\chi}$ vanishes by symmetry, and consequently so does the corresponding weighted constraint Φ, and the remaining constraint $(G^{\rho}{}_{\rho} - G^{\chi}{}_{\chi})$ is guaranteed to be even. A

*) In practice we impose these conditions at a finite, but large $\rho = \rho_{\max}$ and check in Appendix B that the results are independent of $\rho_{\max}$.

similar situation occurs on the $\chi = \pi/2$ boundary for $\rho > 0$ which represents the other periodic boundary. Indeed these periodic boundaries are fictitious in the sense that we can consider the problem on the unwrapped covering space where these boundaries are 'removed', and thus we should not need to impose any constraints here.

For $\chi = \pi/2$, but now with $\rho < 0$, we have the symmetry axis. Again this is in principle a 'fictitious' boundary, but we must impose $C = 0$ here for the elliptic equations, and it is hard to see how this would lift to a covering space with 'no' boundary. For this reason, we examine the situation at the axis in more detail. Using the boundary conditions from the elliptic equations, and assuming the metric components are regular, $G^{\rho}{}_{\chi}$ vanishes there, but $(G^{\rho}{}_{\rho} - G^{\chi}{}_{\chi})$ does not unless the normal gradient of C vanishes. However, since the measure $\det g_{MN}$ vanishes near this axis, both Φ and Ψ are zero, and therefore from the point of view of solving the CR constraint equations, we need do no more here. As discussed in the original implementation of this method,[18] this resolves the paradox that $C = 0$ *and* C has a Neumann boundary condition, despite the fact that we solve C using a boundary value formulation. Whilst we only impose $C = 0$ to be compatible with the elliptic equation behaviour, if we consistently provide data on the *other* boundaries to ensure that the weighted constraints vanish *everywhere*, then this Neumann condition follows automatically, and does not need to be explicitly imposed at the symmetry axis.

Now let us consider the remaining boundaries, the horizon and asymptotic boundary. At the horizon we only have 2 conditions from the elliptic equations and require another to specify the elliptic data. Firstly at the horizon we find that the $G^{\rho}{}_{\chi}$ constraint implies the horizon temperature is a constant,

$$(A - B + C)_{,\chi} \mid_{\rho=\rho_0} = \frac{1}{2}\frac{J_{,\chi}}{J} \mid_{\rho=\rho_0}, \tag{13}$$

and the remaining constraint $(G^{\rho}{}_{\rho} - G^{\chi}{}_{\chi})$ requires,

$$(A - B + C)_{,\rho} \mid_{\rho=\rho_0} = \frac{1}{2}\frac{J_{,\rho}}{J} \mid_{\rho=\rho_0} -1. \tag{14}$$

Lastly, asymptotically at large ρ (or equivalently r), due to the exponential decay of χ (or equivalently z) dependence, the $G^{\rho}{}_{\chi}$ constraint goes exponentially to zero, and so the weighted constraint Φ is guaranteed to go to zero, even though $\det g_{MN} \sim \rho^3$. Due to this power law growth of the measure $\det g_{MN}$, it is less obvious the $(G^{\rho}{}_{\rho} - G^{\chi}{}_{\chi})$ constraint weighted as Ψ goes to zero, as $(G^{\rho}{}_{\rho} - G^{\chi}{}_{\chi})$ (unlike $G^{\rho}{}_{\chi}$) depends on the homogeneous components of the metric, which only decay as a power law. However, the behaviour of the homogeneous component implied by the elliptic equations in (11) does also ensure that $\Psi = 0$ asymptotically.

Now we must decide how to specify data for the elliptic equations (i.e. one condition for each metric function on each portion of the boundary), and also satisfy the constraint problem. With the conditions already required by the elliptic equations, we have sufficient data and $\Phi = 0$ on all boundaries, *except* the horizon. The second weighted constraint, $\Psi = 0$, is satisfied only asymptotically. At the horizon neither

constraint is satisfied, and we require one more condition for a linear combination of A, B and C to make up the elliptic data, as we so far only have (12).

We could impose the constant horizon temperature condition and thus set Φ to zero on the horizon. As we have seen Φ is zero on all the other boundaries, and from the CR relations it obeys a Laplace equation, and therefore this would uniquely set it to zero everywhere. Ψ would then be zero following from the CR relations and the fact it vanishes asymptotically.

However it is numerically more stable to impose the $(G^{\rho}{}_{\rho} - G^{\chi}{}_{\chi})$ constraint, and hence $\Psi = 0$ at the horizon instead. The $(G^{\rho}{}_{\rho} - G^{\chi}{}_{\chi})$ constraint is a typical elliptic boundary condition, whereas imposing the constant horizon temperature $G^{\rho}{}_{\chi}$ constraint involves 'less local' tangential derivatives on the horizon. Now we have sufficient data to impose both constraints globally via the CR problem. Since at the horizon $\Psi = 0$, Φ has a Neumann condition there, and it is zero on all other boundaries. Hence it will be zero everywhere, as it obeys the Laplace equation. The CR relations then imply that Ψ is constant, and it must be zero, as it was imposed to be zero on the horizon.

2.4. *How ρ_0 specifies the size of the black hole*

Taking $A, B, C \to 0$ asymptotically, and thus the asymptotic compactification radius to be $L = \pi$, there must be one constant entering the boundary data that specifies the size, or the mass of the black hole. Intuitively one would imagine this to be ρ_0 as this certainly enters into the boundary data at the horizon, in Eqs. (12) and (14).

To confirm this, we must demonstrate that ρ_0 is a physical quantity, not simply a coordinate artifact. Thus we must show that there is no residual coordinate transformation (i.e. conformal transformation on ρ and χ) that preserves the rectangular boundaries, the conditions on these boundaries, and the asymptotic radius of compactification, but changes the effective ρ_0 in the new coordinates. If this were the case, ρ_0 would not correspond to a physical parameter, and therefore could not specify the size of the black hole, which certainly is a physical parameter.

Let us suppose we have a black hole solution with a particular ρ_0. Now let us construct the most general coordinate transformation that simply preserves the rectangular boundaries. We construct new coordinates as $\rho \to \tilde{\rho} = \tilde{\rho}(\rho, \chi)$ and $\chi \to \tilde{\chi} = \tilde{\chi}(\rho, \chi)$, and then must solve a CR problem to build the conformal coordinate transformation. Let us do this by specifying data for the Laplace equation that determines $\tilde{\chi}$. For the boundaries to remain rectangular, we must specify a constant $\tilde{\chi} = \tilde{\chi}_0$ on the $\chi = 0$ boundary and constant $\tilde{\chi} = \tilde{\chi}_{\pi/2}$ on the $\chi = \pi/2$ boundary. At the horizon, we must specify a Neumann condition on $\tilde{\chi}$ and then the CR equations guarantee that $\tilde{\rho}$ is constant there. Regular asymptotics then give the unique solution

$$\tilde{\chi} = \tilde{\chi}_0 + \left(\tilde{\chi}_{\pi/2} - \tilde{\chi}_0\right) \frac{\chi}{\pi/2}. \tag{15}$$

This solution now completely determines $\tilde{\rho}$ up to a further constant of integration.

Now that we have the general transform preserving the rectangular boundaries, let us further restrict it by making it preserve our boundary conditions. Firstly,

since $\tilde{\chi}_0$ does not enter into any equation or boundary condition, we may freely set it to zero. Secondly, since we have selected $A, B, C \to 0$ asymptotically, we require $\tilde{\chi} = \pi/2$ on the $\chi = \pi/2$ boundary if we are not to change the compactification radius $L = \pi$. Thus now, $\tilde{\chi} = \chi$. This implies from the CR relations,

$$\tilde{\rho} = \delta\rho_0 + \rho, \tag{16}$$

where $\delta\rho_0$ is a constant of integration.

However there is a subtle point. Whilst ρ_0 only enters the boundary conditions explicitly at the horizon, the boundaries conditions change on the $\chi = \pi/2$ axis for $\rho > 0$ (where C has a Neumann condition imposed) to $\rho < 0$ (where $C = 0$ is imposed). Since we have fixed this transition of the boundary conditions to occur at $\rho = 0$ in the new coordinates, this will occur at $\tilde{\rho}_0 = \delta\rho_0$. Hence, the transformed solution will *not* satisfy*) the boundary conditions in the new coordinates where this transition now occurs at $\tilde{\rho} = 0$. Thus, due to our fixing the transition from the symmetry axis to periodic boundary at $\rho = 0$, there are no residual coordinate transformations mapping solutions with horizon position ρ_0 to a transformed solution, solving the boundary conditions but with a different horizon position $\tilde{\rho}_0$ in the new coordinates. Therefore ρ_0 does indeed specify the physical size of the black hole.**)

2.5. *Thermodynamic quantities*

We compute the temperature $\mathcal{T}$ and entropy $\mathcal{S}$ of the black hole solutions. These are given as

$$\begin{aligned} \mathcal{T} &= \frac{1}{2\pi}\frac{3e^{A-B+C}}{2^{5/3}\sqrt{J}}\,|_{\rho=\rho_0}, \\ \mathcal{S} &= \frac{1}{4}\left[2e^{4B_{bg}}\int d\Omega_3\int_0^{\pi/2} d\chi\sqrt{J}r^3 e^{4B+C}\right]_{\rho=\rho_0}. \end{aligned} \tag{17}$$

*) Note that if the physical solution had $C = 0$ and $C_{,\chi} = 0$ on the entire $\chi = \pi/2$ boundary, then ρ_0 would *not* specify the solution. As discussed the constraints ensure that whilst we only impose $C = 0$, C also satisfies a Neumann condition on the symmetry axis, $\rho < 0$ and $\chi = \pi/2$. However, for $\rho > 0$ on the periodic boundary, we only impose a Neumann condition and there is no reason why C would vanish there too. Indeed in the solutions we find C does not vanish there, although it is very small.

**) It is interesting to note that the horizon must have spherical topology for this argument to work. If we were considering a string horizon, and thus chose $\rho_0 > 0$, then the boundary conditions would simply be Neumann all along the $\chi = \pi/2$ boundary, and the new transformed solution in the $\tilde{\rho}, \tilde{\chi}$ coordinates would satisfy all our boundary conditions, but with a different value of $\tilde{\rho}_0$ ($\neq \rho_0$) on the horizon. It is for this rather subtle reason that the boundary conditions in the non-uniform string case of Ref. 12) must be imposed differently, using the $G^{\rho}{}_{\chi}$ constraint equation on the horizon (rather than $(G^{\rho}{}_{\rho} - G^{\chi}{}_{\chi})$ as we use here) which, being a tangential condition, rather than a condition on the normal derivatives, introduces a new integration constant that parameterises the mass (or equivalently λ) for the string solution. The fact that this is a tangential condition appears to make the algorithm 'less local' and to require considerable under-relaxation, whereas here we do not need this. However, here while we need not damp the relaxation, the exposed $\rho < 0$ symmetry axis does lead to the coordinate singularity induced stability problems discussed above.

The mass may be computed by two independent methods. Firstly we may determine the mass from the asymptotics of the metric as

$$M = \frac{\pi L}{4}\left(-3a_2 - b_2 + c_2\right), \tag{18}$$

using the expansions (11).[54] Secondly the mass may be determined by integration from the First Law, using $dM/d\rho_0 = \mathcal{T}(\rho_0)d\mathcal{S}/d\rho_0$ (which applies for fixed asymptotic compactification radius — see below) along the branch of solutions, and taking $M = 0$ for $\rho_0 \to -\infty$ to define the integration constant. Later (see Fig. 9) we see very good agreement between these two values. This is a good indication that the elliptic equations are well satisfied globally and the boundary conditions are imposed correctly. An important point is that the First Law does *not* test whether the constraint equations $G^r{}_z, (G^r{}_r - G^z{}_z)$ are satisfied, and we elaborate on this point in Appendix C. Since we completely relax the elliptic equations, it is then not terribly surprising that the First Law holds very well. What is absolutely essential is that the constraints are also checked, to ensure they are well satisfied. They indeed are, as seen from the tests outlined in Appendix B.

Since the black hole geometries are compactified, the mass is not the only asymptotic charge. This feature, shared more generally by branes, was originally discussed in Ref. 55), and more recently in relation to the black hole/black string problem in Refs. 26)–28). It is easy to see there must be another charge. As the geometry becomes homogeneous at large distances from the symmetry axis, it can be dimensionally reduced to Einstein-dilaton-Maxwell theory. For our regular static solutions, the Maxwell vector can always be gauged away, but we are left with gravity and the dilaton scalar, indicating that we should consider not only an asymptotic mass, but also a scalar charge.

From a purely 6-dimensional point of view, the second charge can be thought of as a binding energy per unit mass, n, resulting in a modified First Law,

$$dM = T\,dS + n\,M\,\frac{dL}{L}, \tag{19}$$

with the new term representing the work done when varying the asymptotic size of the extra dimension. In our solutions, fixing L we reproduce the usual form of the First Law for black holes. However, we may determine n from the asymptotics of the metric, or from the Smarr relation,

$$TS = \frac{3-n}{4}M, \tag{20}$$

again discussed in Ref. 55), and given explicitly for the problem at hand in Refs. 26) and 27), where n was calculated from the asymptotics to be

$$n = \frac{a_2 + 3\,b_2 - 3\,c_2}{3\,a_2 + b_2 - c_2}. \tag{21}$$

As emphasised in Ref. 27) we may use the Smarr formula as a check of our numerics. This is very similar to the First Law check discussed above, which only involves the

mass, whereas Smarr's law involves both M and n. It is important to note that for the same reasons the First Law does not probe the constraint equations, the Smarr formula also does not. Thus again it is no replacement for the checking of constraint equation violations we perform in Appendix B.

2.6. *Behaviour of the method*

Following the above method, we may construct a unique numerical solution for each value of ρ_0. The elliptic equations can be solved very stably, once the coordinate induced instability at the axis is dealt with (see Appendix A). Since we have designed the coordinates and method to have $A, B, C \to 0$ in the small black hole limit $\rho_0 \to -\infty$, the method behaves well in this limit. As the black hole becomes larger, so that ρ_0 is finite and negative, A, B and C deviate away from zero, although they remain regular as we expect. The topology of the ρ coordinate dictates

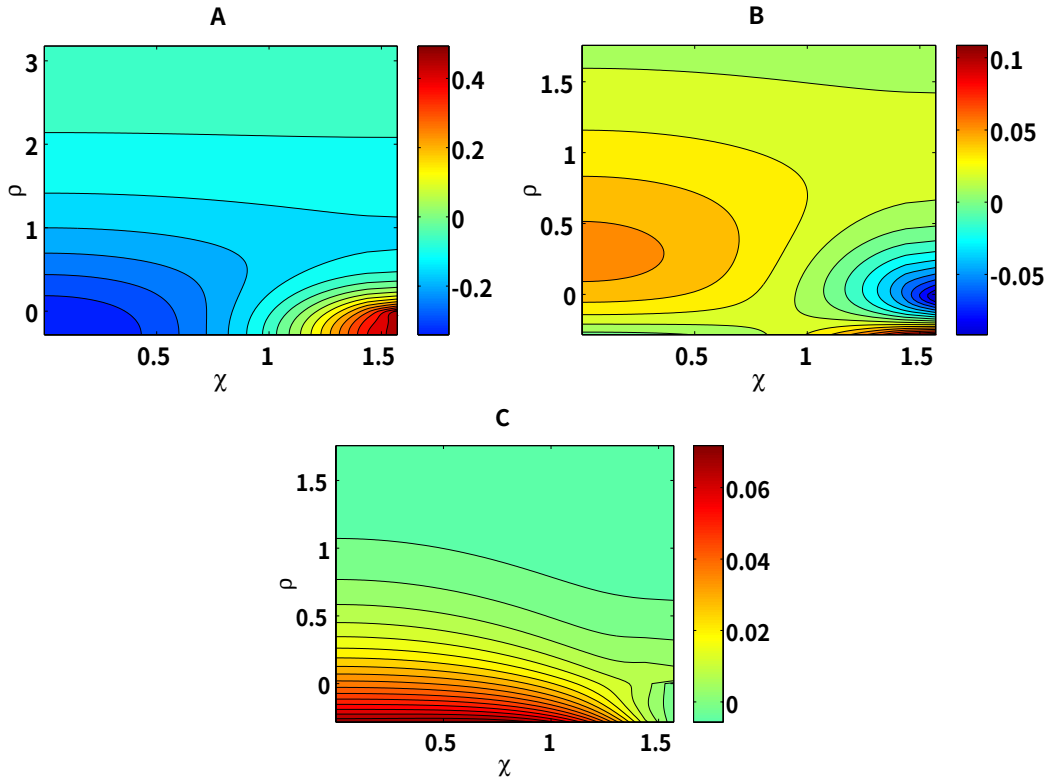

Fig. 3. Plots of the metric functions A, B and C for a black hole solution with $\rho_0 = -0.28$. This is quite near to the maximal size ($\rho_0 = -0.18$) that we are able to construct before we become limited by gradients and lattice resolution near the symmetry axis at $\chi = \pi/2$ for $\rho < 0$. Already this black hole solution has a horizon volume and mass that are equal to those of the most non-uniform strings compactified on the same asymptotic radius. Whilst the lattice is large, being 140×420 in χ, ρ, since ρ_0 is very close to zero the number of points along the symmetry axis is only around ~ 20. This is still enough to see good behaviour in the metric functions. Note that B and C are much less than A in magnitude. The maximum ρ for the lattice is ~ 5, and not all the domain is shown as the functions simply go smoothly to zero at large ρ.

$\rho_0 = 0$ is the largest black hole that could exist. Using reasonable resolutions (up to $\sim 140 \times 420$), we were able to find solutions with a maximum $\rho_0 \simeq -0.18$, yielding a black hole horizon with typical radius comparable to the asymptotic compactification radius. As an example we show the metric functions A, B and C for $\rho_0 = -0.28$ in Fig. 3. Note that the magnitude of C is much less than that of A and B, and this is increasingly true the smaller the black hole. Hence the spatial sections are approximately conformally flat.

The larger the black hole is, the larger the gradients in the metric functions, and for a fixed resolution the method no longer converges past a certain black hole size. Going to a higher resolution we find the problem is removed, and the size can be further increased, but obviously the problem then reappears at a new larger size. The key area where we lack resolution is near the symmetry axis. For the large black holes, with ρ_0 closer to zero, there become fewer and fewer points there. With the maximum size we could find, $\rho_0 = -0.18$, so the coordinate distance of the symmetry axis is 0.18, compared to the coordinate distance along the horizon which is $\pi/2 \sim 1.6$, and hence with our simple discretization scheme (see Appendix A for details) the axis is allocated far fewer points. The closer ρ_0 gets to zero, the more acute this problem. Thus in our simple numerical implementation, we are limited by resolution, and hence computation time. We present results in this paper obtained using modest resources and simple relaxation algorithms. It is likely that with improvements in both areas one can achieve far improved data. For example, adaptive grid methods may allow us to circumvent the lack of resolution near the symmetry axis, but it is a serious challenge to implement these and maintain a stable relaxation algorithm. However, already with our simple implementation it is possible to derive interesting physical results as we shall see.

§3. Results

The questions we wish to address are whether there is an upper mass limit for these solutions, and whether the geometry is compatible with continuation to the non-uniform string branch. Whilst $\rho_0 = 0$ is the largest black hole due to the topology of the (ρ, χ) coordinate system, obviously the metric functions A, B and C may diverge in this limit, and consequently so might the horizon volume and mass, and thus a priori we have no reason to assume such an upper mass limit will exist. On physical grounds, one could argue that a black hole would not be able to 'fit' into the compact extra dimension, but we stress that in the unstabilised pure Kaluza-Klein theory it is only the asymptotic radius we have fixed for the branch of solutions, and there is nothing to prevent the geometry along the axis and horizon from decompactifying as the black hole becomes larger.

3.1. *Horizon geometry*

In order to approach these questions we embed the *spatial* horizon geometry into 5-dimensional Euclidean space,

$$ds^2 = dX^2 + dY^2 + Y^2 d\Omega^2_{(3)}. \tag{22}$$

Then, matching our geometry at $\rho = \rho_0$ implies that

$$Y(\chi) = r\, e^{\beta + \frac{2}{3}\gamma}\,|_{\rho=\rho_0},$$
$$X(\chi) = \int_0^{\chi} d\chi' \sqrt{\left[J(\chi')\, e^{2(\beta-\gamma)(\chi')} - (Y_{,\chi'})^2\right]}_{\rho=\rho_0}, \tag{23}$$

and we interpolate the numerical data to perform the integral. Clearly for small black holes, we expect a spherical horizon, and for larger black hole, we expect deformation. We find excellent agreement with the horizon being a prolate ellipsoid for all our solutions up to the maximum size available $\rho_0 = -0.18$. In Fig. 4 we plot a moderate and a large black hole to demonstrate the accuracy of the ellipsoid fit. We plot the positions of the actual lattice points in the embedding coordinates, X and Y, for our highest resolution, and against these we plot the fitting ellipse, and note that all the points fall consistently on the fit curve. Thus from now on it is easier for us to characterise the geometry using the major (polar) and minor (equatorial) axis radii, which we term $R_{\rm polar}$ and $R_{\rm eq}$. Then using this elliptical fit we plot the ellipse radii and ellipticity,

$$\epsilon = \frac{R_{\rm eq}}{R_{\rm polar}}, \tag{24}$$

against ρ_0 for all our solutions in Fig. 5. We see that for the largest black holes the ellipticity decreases to only ~ 0.87, even though the ellipsoid radius $R_{\rm polar}$ increases to ~ 1.5, which is approximately the size of the asymptotic compactification half-period $L/2 = \pi/2$. Thus it is clear from the prolateness and lack of deformation that the geometry around the symmetry axis is decompactifying.

We now wish to characterise this decompactification. In Fig. 6, we plot a selection of black hole embeddings, now including the embedding of the symmetry axis to show its proper length. Note that we only show half of the full period, and thus reflecting the horizon and axis about $X = 0$ generates the full compact period. The asymptotic compactification radius for half the period is $L/2 = \pi/2$ here. We term the length of the axis for half the period, $L_{\rm axis}$, and it is given by

$$L_{\rm axis} = \int_{\rho_0}^{0} d\rho J e^{\beta-\gamma}\,|_{\chi=\pi/2}\,. \tag{25}$$

We see that $L_{\rm axis}$ decreases in these figures for larger black holes, but the horizon radii increase more rapidly, resulting in an overall decompactification. In Fig. 7 we show the maximum value of the embedding coordinate X to contain half a period of both the horizon and the symmetry axis,

$$X_{\rm max} = X(\pi/2) + L_{\rm axis}, \tag{26}$$

which is essentially the same as $(R_{\rm polar} + L_{\rm axis})$ since the ellipse is such a good fit to the horizon geometry. We take this quantity to be the physically relevant (and coordinate invariant) measure of the compactification length near the axis.

These plots clearly show the axis decompactifying. Since we are only able to 'grow' black holes to $\rho_0 = -0.18$, it is unclear whether; i) there exists a maximal

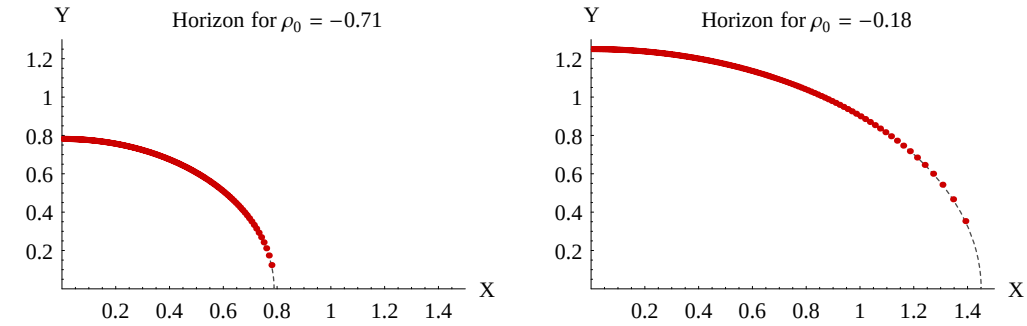

Fig. 4. Embedding of horizons into Euclidean space for a moderate black hole on the left, with $\rho_0 = -0.71$, and the maximal black hole on the right with $\rho = -0.18$. Whilst we interpolate the numerical functions to determine the embedding, we plot here the actual positions of the lattice points for our highest resolution to give an indication of how the resolution varies with position on the horizon. For all the solutions, we may fit a prolate ellipsoid to the horizon, the dashed line, and in all cases we find perfect agreement.

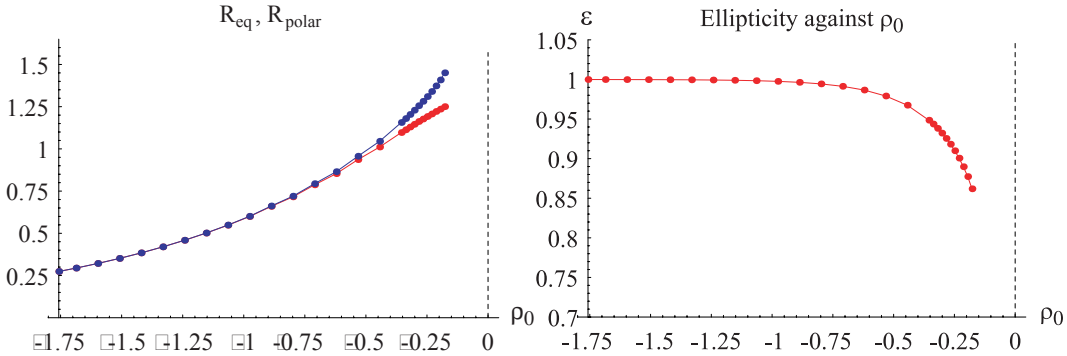

Fig. 5. On the left we plot the equatorial and polar radii of the ellipses fitted to the horizon embeddings, against the parameter ρ_0 specifying the size of the black hole. It is unclear what happens in the limit $\rho_0 \to 0$ where the ρ coordinate changes topology. It would be very interesting to know if $R_{\rm eq}, R_{\rm polar}$ remain finite or not, and thus whether there is a maximum mass black hole or not. Since the geometry near the axis and horizon decompactifies, even though the largest black holes found have radii comparable to the corresponding asymptotic half period distance $L/2 = \pi/2$, the horizons are still quite spherical. We plot the ratio of the radii in the right-hand diagram. Again it is unclear what will occur in the limit $\rho_0 \to 0$.

mass black hole, or ii) whether the decompactification continues in such a way that arbitrarily large black holes may exist, e.g. with $L_{\rm axis} \to 0$ or a constant in the limit of infinite mass. If there were a maximum mass, it seems likely from the figures that ρ_0 can still be increased some way more before we would expect to reach it.

3.2. *Comparison with non-uniform strings*

We now compare these geometries with those of the critical uniform string ($\lambda = 0$), and the most non-uniform strings ($\lambda \simeq 4$) found in Ref. 12), rescaling

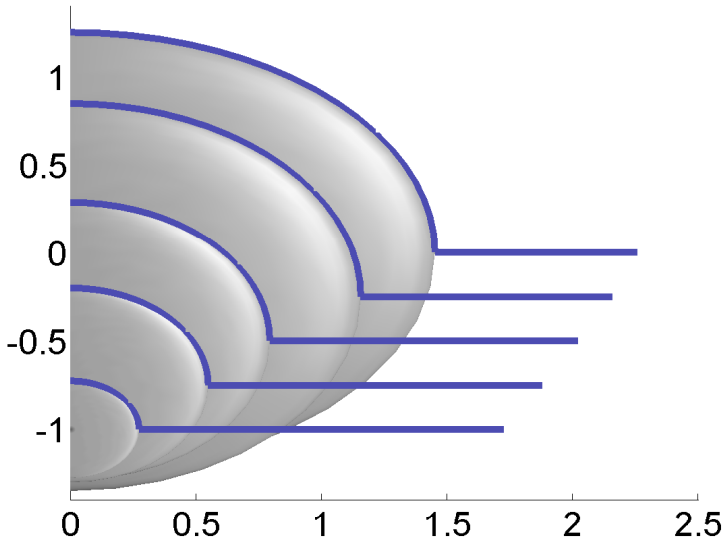

Fig. 6. We show both the embedding of the horizon, and also the symmetry axis for various solutions ranging up to the largest black hole found. These embeddings are for half a period, and should be reflected about $X = 0$ to obtain the full geometry. The asymptotic radius of this half period is $L/2 = \pi/2$. We clearly see that the total space taken up by the solutions in the embedding X coordinate grows as the black hole increases in size, despite the fact that the symmetry axis decreases in length, indicating that the overall geometry near the horizon and axis decompactifies. We also see that even the largest black hole still appears to have considerable 'room' to increase its size still further.

the asymptotic radius appropriately, and defining λ as in that paper,

$$\lambda = \frac{1}{2}\left(\frac{R_{\max}}{R_{\min}} - 1\right), \tag{27}$$

where $R_{\max,\min}$ are the maximum and minimum horizon radii, respectively. Whilst $\lambda = 3.9$ was the most non-uniform string found there, the geometry and also thermodynamic quantities $M, \mathcal{T}$ and $\mathcal{S}$ appear to asymptote for large λ (see also Ref. 29)) and thus the $\lambda \to \infty$ values are expected to be very similar to those at $\lambda \simeq 4$, probably only differing by a few percent. Strong evidence for this comes from the realization that a conical geometry forms at large λ, as tested in Ref. 30). Once λ is relatively large, say $\lambda \sim 2$, only the geometry near the string 'waist' appears to change with increasing λ as the cone forms. With the rescaling so that the asymptotic radius for one period of the solution is $L = \pi$, we find the following values,

$$\begin{aligned} \text{Critical string} \qquad R_{\max,\lambda=0} &= 0.64, \\ X_{\max,\lambda=0} &= \frac{\pi}{2}, \\ M_{\lambda=0} &= 1.47, \\ \mathcal{T}_{\lambda=0} &= 0.250, \end{aligned}$$

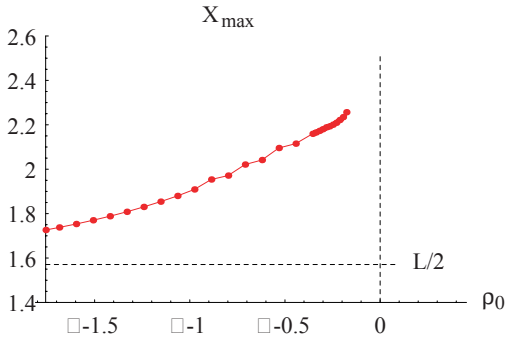

Fig. 7. Plot showing $X_{\max}$, the 'length' taken up by half the horizon and the symmetry axis when embedding into Euclidean space. This quantity offers a physical and coordinate invariant measure of the radius of compactification near the horizon. We see that as the black hole grows with increasing ρ_0, the axis decompactifies considerably. Again, it is unclear what happens in the $\rho_0 \to 0$ limit.

$$\mathcal{S}_{\lambda=0} = 3.99.$$

Highly non-uniform string

$$\begin{aligned} R_{\max,\lambda=3.9} &= 1.11, \\ X_{\max,\lambda=3.9} &= 1.91, \\ M_{\lambda=3.9} &= 3.38, \\ \mathcal{T}_{\lambda=3.9} &= 0.184, \\ \mathcal{S}_{\lambda=3.9} &= 12.94. \end{aligned} \tag{28}$$

Here $R_{\max,\lambda}$ is the maximal radius of the horizon, and $X_{\max,\lambda}$ is again the maximum value of X when embedding half a period of the strings into Euclidean space, using the metric (22) as for the black holes, and taking $X = 0$ at the maximal radius of the horizon, so that $X = X_{\max}$ at the 'waist', the minimum radius. Now, there is no exposed symmetry axis, and therefore $X_{\max}$ is just the change in X when traversing the horizon for a half period. As noted in Ref. 29) the proper distance (which is not equal to the embedding coordinate X) along the horizon increases with λ indicating that the geometry decompactifies there.

The key observation of this paper is now evident from the previous plots of the embedded black hole geometry. Already for $\rho_0 \simeq -0.35$ we see the black hole equatorial radius R_{eq} is equal to $R_{\max}$ for the highly non-uniform string ($\lambda = 3.9$), which as stated above we take to be approximately equal to $R_{\max}$ in the limit $\lambda \to \infty$. As ρ_0 increases past this point, the black holes continue to become larger in radius. In addition we see from $X_{\max}$ that the geometry along the axis has decompactified as much as that of the very non-uniform strings for even quite small black holes with $\rho_0 \simeq -1.0$, and again the trend seems to continue for increasing ρ_0 past this point. The implication is clear, that it seems difficult to imagine black hole solutions making a transition at $\rho_0 = 0$ via a cone geometry to the most non-uniform strings, as they simply become 'bigger' than the most non-uniform strings already for $\rho_0 \simeq -0.35$. We may gain more insight into this result in Fig. 8 by plotting the embedding of

the $\lambda = 3.9$ non-uniform string, and the largest black hole relaxed ($\rho_0 = -0.18$) into Euclidean space, including the symmetry axis of the black hole. Again we note that with increasing λ past 3.9 we only expect the geometry in the cone region to change, and thus the geometry of the $\lambda = 3.9$ string should be very close to that of the limiting string at $\lambda = \infty$ (see Ref. 29) for curves of $R_{\max}$ against λ).

Whilst we earlier claimed that resolution becomes limited near the horizon and axis for large black holes, we find that the values of $R_{\rm eq}$ and $R_{\rm polar}$ only vary by $\sim 1\%$ when the resolution is doubled from 70×210 to our highest resolution 140×420 for the solution with $\rho_0 \simeq -0.35$ that parallels the most non-uniform string horizon size. The length along the axis $L_{\rm axis}$ varies only a little more, approximately $\sim 3\%$. Thus while decreasing the axis resolution and increasing the black hole size limits the ability of the algorithm to converge, the resolution is still high enough for the accuracy of our large black hole solutions to be high. For further comparison of quantities measured at different resolutions, see Fig. 9 and Appendix A.

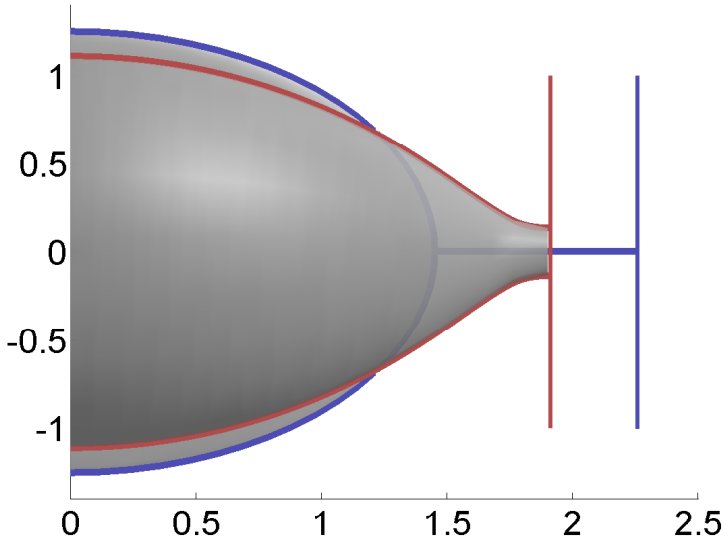

Fig. 8. An illustration of the intrinsic geometries of the maximum size black hole found ($\rho_0 = -0.18$) compared to a highly non-uniform string ($\lambda = 3.9$) whose geometry is expected to be very close to the limiting $\lambda = \infty$ solution, with a conical geometry near the waist of the horizon. Only half a period of the solutions is shown, and for the full geometry one should reflect about $X = 0$. Both are taken to have an asymptotic compactification half period $L/2 = \pi/2$. We see immediately that the black hole is simply 'bigger' in all aspects. It has a larger equatorial radius, and including the exposed symmetry axis, it takes up more 'room' in the X direction — i.e. it has decompactified more. Indeed, we also find it has a larger mass and lower temperature. Furthermore, it looks very much as if we can increase the black hole size further still. The implication is that the $\lambda = \infty$ string solution presumably cannot be connected (through a conical topology change) to *this* branch of black hole solutions.

3.3. *Thermodynamics*

Now we turn to the thermodynamic quantities to see whether our comparison of the black hole/string horizon intrinsic geometry is paralleled in these independent observables. We might now reasonably expect the mass of the black holes to become greater than that of the most non-uniform strings, and the horizon temperature to become less. In Fig. 9 we plot the temperature, $\mathcal{T}$, and mass M of the black hole solutions, now against the horizon entropy $\mathcal{S}$. The mass is computed in two ways, firstly asymptotically from the metric [see Eq. (18)], and secondly by integration from the First Law. We clearly see very good agreement for these as expected. As discussed earlier in §2.5, this is a good test of the elliptic equations, but does not test the constraints which are the really important quantities to check for this elliptic method, as they are not imposed directly. These constraints are tested explicitly in Appendix B.

On these plots we also show the same quantities for the non-uniform string branch up to $\lambda = 3.9$. Again we emphasise that the $\lambda = 3.9$ point probably lies very close to the $\lambda = \infty$ point on this diagram. Our expectations are confirmed, with the temperature decreasing, and the mass increasing beyond those for the most non-uniform strings already by $\rho_0 \simeq -0.30$, and the trend continuing for larger ρ_0, again reflecting the fact that the black holes become 'bigger' than the non-uniform strings. We also plot the behaviour of a 6-dimensional Schwarzschild solution, and find that since the axis is decompactifying, and as a consequence the black hole horizon geometry is only slowly deforming from a sphere, the black holes closely reproduce this Schwarzschild behaviour.

There is one further point we may observe from these plots. The non-uniform branch presumably terminates at $\lambda = \infty$, very close to the $\lambda = 3.9$ solutions plotted. Therefore the whole non-uniform branch of solutions $\lambda = 0$ to ∞ appears to lie very close to the black hole curves both in $\mathcal{M}$ and $\mathcal{T}$ against $\mathcal{S}$. Since the branches do not appear to connect, we can think of no particular reason why this should be so, and presumably it is just an interesting coincidence.

Finally we turn to the last (and truly higher-dimensional) thermodynamic quantity, the binding energy n of our solutions. This turns out to be very small, and thus prone to numerical error. Referring back to (21) we recall that n is given by a ratio of asymptotic quantities, with numerator $3\,b_2 - 3\,c_2 + a_2$. In Fig. 10 we plot the magnitudes of both a term in the numerator, and the numerator itself, and demonstrate that the numerator is relatively very small, $\sim 10\%$ of the terms making it up, indicating cancellations occur between the terms. This is a problem numerically since the asymptotic quantities a_2, b_2 and c_2 are already difficult to measure, and thus quantities depending on detailed cancellations between them certainly should not be trusted. A further caveat is that for small black holes both the numerator and denominator are small, and their ratio is consequently extremely unreliable. Computing n from the asymptotics, we find its value to be less than ~ 0.1 for these solutions, but the errors appear large, and we stress simply that it is small, and we do not feel we can give its value with certainty here. We may reassure ourselves that whilst n is 'noisy' due to numerical error, this is simply because n is close to

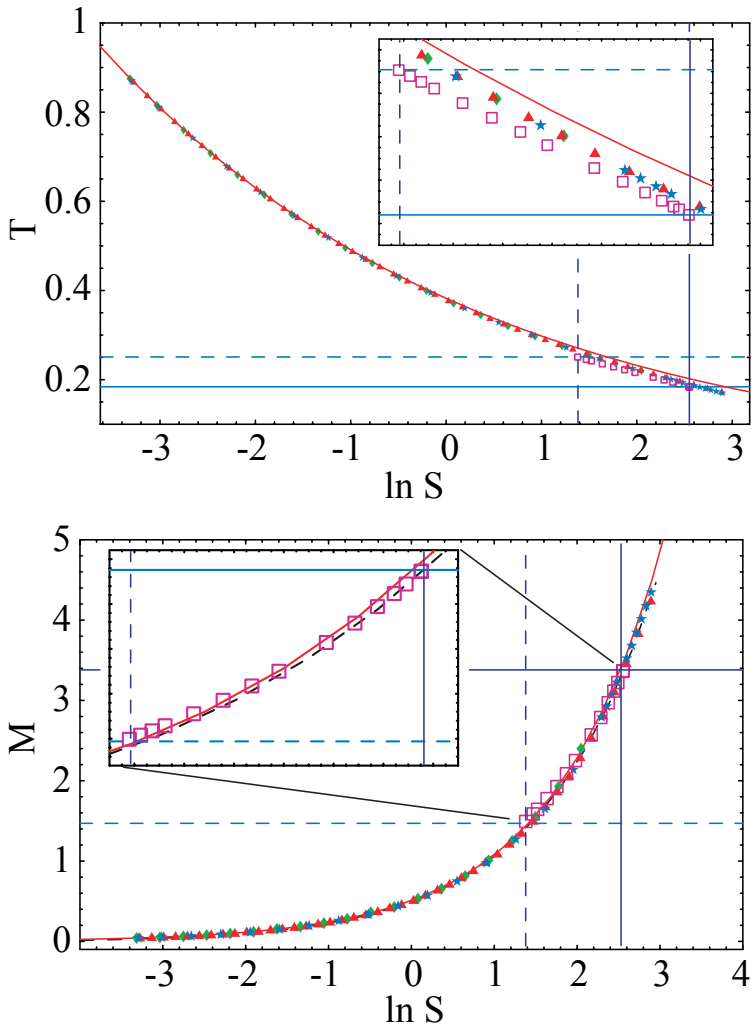

Fig. 9. Plot showing the black hole temperature $\mathcal{T}$ and mass M against entropy $\mathcal{S}$ calculated by Eqs. (17) and (18). Three resolutions for the black holes are used, 36×106 (diamond), 70×210 (triangle) and 140×420 (star), and excellent consistency is found. In the figure for the mass, the dashed line gives the mass computed by integrating the First Law, showing excellent agreement with the asymptotically measured mass. The solid lines represent the behaviour of a 6-dimensional Schwarzschild solution, and for these black holes, despite the fact that their size becomes equivalent to the compactification radius, we see little deviation from this. We also show the same quantities plotted for the non-uniform strings as pink open squares. The dashed and solid straight lines show the limiting values for $\lambda = 0$ and $\lambda \to \infty$. We include magnifications of the regions where the non-uniform strings exist. Interestingly, the non-uniform values lie very close to the black hole curves, although this appears simply to be a coincidence.

vanishing, and Smarr's law is extremely well satisfied. Also in Fig. 10 we plot the two sides of the Smarr relation (20), TS and $(3-n)M/4$, against ρ_0. In addition, we also plot $3M/4$, setting $n = 0$, on the same plot. It is seen to lie so close to the curve with the actual measured n that it is clear n is quantitatively small, and furthermore

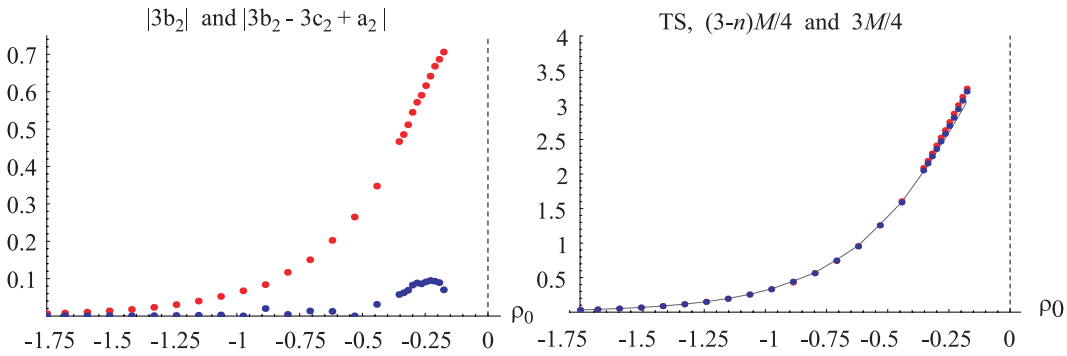

Fig. 10. (Left) A plot of the magnitude of a term in the numerator of n, the binding energy, and the magnitude of the numerator itself. We see this numerator is $\sim 10\%$ of the value of one of its constituent terms, and thus detailed cancellations occur, and the value of n is very small. Since the asymptotic quantities a_2, b_2 and c_2 are already difficult to compute accurately, we should not trust a numerical quantity that depends on detailed differences of these, and thus is very small in comparison. (Right) A plot of the left- (TS as a solid line) and right-hand ($(3-n)M/4$) as black points) sides of Smarr's formula, confirming that whilst n is very hard to determine accurately, Smarr's formula is very well satisfied by our data. To confirm that n is indeed extremely small, we show the right-hand side computed with $n = 0$, i.e. $3M/4$ as gray points, which gives a slightly worse fit, but only marginally.

we cannot currently expect to measure it with any accuracy as argued above. Much higher precision would be required for this, and thus we leave determining the actual (small) values of n for a future work.

§4. Discussion and outlook

We have shown that static black holes in pure 6-dimensional gravity compactified on a circle, i.e. Kaluza-Klein black holes, may be found using elliptic numerical methods. As expected, for a fixed asymptotic compactification radius, the small black holes behave as 6-dimensional Schwarzschild solutions. As they grow the geometry on the axis decompactifies relative to the fixed asymptotic radius, and the horizon deforms into a prolate ellipsoid. Since we are limited by numerical resolution, we are currently unable to probe whether the axis decompactifies indefinitely, and consequently black holes of any mass can be found, or whether instead there is an upper mass limit for the black holes. This is clearly an interesting issue to resolve in future work.

The most interesting result we find is that whilst we are only able to compute black holes whose radii become approximately equal to the asymptotic compactification radius, these are already sufficiently large that they are simply 'bigger' than the most non-uniform string solutions constructed in Ref. 12), both in terms of horizon volume and mass. For the largest black hole solutions we found the horizons are still quite spherical since the axis geometry decompactifies, making 'room' for the horizon. It therefore appears that they should be able to further increase in size and mass, past the point where we are currently able to construct them, before

any possible upper mass limit would be reached. Given these results, it therefore seems rather unlikely that this black hole branch of solutions can merge with the non-uniform strings via a conical geometry developing in the polar regions of the horizon, as suggested by Kol.[23] This is despite the fact that we have excellent numerical evidence that the highly non-uniform strings do indeed exhibit the required conical geometry at their waist, which previously lent weight to this conjecture.[30]

This is then very interesting geometrically, and raises the obvious question of whether the static non-uniform string solutions can be continued through the $\lambda \to \infty$ solution with its conical waist to a *new* branch of black hole solutions. Obviously while these would have horizons that do not wrap the extra coordinate, they would be distinct solutions from those we construct here, and at low mass (if they have a low mass limit) would presumably not look like the 6-dimensional Schwarzschild solution.[*] Similarly, if the black hole branch we partially construct here does turn out to have an upper mass limit, can this branch of solutions be continued through to a new string solution, distinct from that connected to the Gregory-Laflamme critical uniform string? We refrain from speculating on these questions (see the recent paper[28] for an interesting discussion of a variety of possibilities), deferring these issues until improved numerics can be performed that confirm the current results, and can extend the range of these elliptic methods so that these questions may be tackled directly. We do make one further general comment here. As we have seen comparing the work here with the previous work constructing the non-uniform string solutions,[12] the fact that the axis of symmetry is exposed for the black hole solutions completely changes the boundary conditions imposed on the problem. Thus, without proof, it would be dangerous to assume that continuation of a branch of solutions through a topology change in a conical region must always be possible.

Whilst our computations were performed in 6 dimensions, in order to make contact with previous work constructing the non-uniform strings, it would be good to check whether the same behaviour occurs in 5 dimensions. Whilst the difference between 4 dimensions and more than 4 is very large, due to the additional curvature terms entering the Einstein equations from the rotation group of the axial symmetry, the difference between 5 and 6 dimensions is simply in the coefficients entering these equations. Hence, we would be very surprised if the 5 and 6-dimensional systems behaved qualitatively differently, but to be sure, it would be good to check this point by constructing non-uniform strings and black hole solutions in 5 dimensions and comparing them.

Our findings appear to be strongly related to the decompactification of the geometry near the horizon and axis. The reason the black holes become larger than the non-uniform strings is because the axis decompactifies making room for them. Therefore in order to make contact with realistic phenomenology, and thus really determine whether there are interesting strong gravity effects of compactification, it is clearly important to consider the problem again, but include some radius stabilis-

[*] For example the non-uniform string branch may join a branch of black holes that then undergoes additional topology changing, and so in the limit of small mass the horizons are Schwarzschild-like, but with more than one horizon per compactification period.

ing mechanism. Presumably, once stabilisation is included, an upper mass limit for the black holes should be inevitable as the axis cannot decompactify so easily. This is a sufficiently important phenomenological question that this should be checked explicitly, rather than just assumed, as if it turned out not to be true, or only to be true for certain stabilisation mechanisms, this might provide new physical and observational constraints on compactifications that are totally independent of the familiar weak field constraints. It may also provide an important testing ground for the non-linear dynamics of stabilisation mechanisms. Additional matter, such as is required for stabilisation, simply adds elliptic equations to the problem, and no further constraints, and thus in principle can be easily incorporated. We note that, at least with weak stabilisation, the Gregory-Laflamme instability will occur as usual. Hence non-uniform string solutions will also exist, although of course it is not obvious that they can be deformed to have a conical region of their horizon as in the unstabilised case. If they do behave in the same manner as for the unstabilised theory, and if, since the axis could not decompactify readily, the black holes are forced to have an upper mass limit at a lower mass than those probed in this paper, then possibly the topology change to the black hole branch that Kol suggests could occur after all.

Acknowledgements

We would like to thank Troels Harmark, Takashi Nakamura, Jorge Pullin, Harvey Reall and Takahiro Tanaka, and in particular Barak Kol and Evgeny Sorkin for interesting and valuable discussions. Also discussions during and following the YITP workshop YITP-W-02-19 were useful. TW would like to thank YITP, Kyoto and in particular Takahiro Tanaka for much hospitality whilst some of this work was completed. HK is supported by the JSPS and a Grant-in-Aid for the 21st Century COE, and TW was supported by Pembroke college, Cambridge for most of the duration of this project. Numerical computations were carried out at the Yukawa Institute Computer Facility.

Appendix A

Numerical Details

As in previous works[12),18),19)] we use a simple Gauss-Seidel method with second order differencing to relax the elliptic equations. The non-linear source terms are fixed, the resulting Poisson equations are relaxed, and then the sources are updated with the new solutions, and the boundary conditions are refreshed. Repeating this, the elliptic equations are either *completely* relaxed and we find a solution, or convergence is lost at some point early in the relaxation, and all the metric functions diverge dramatically, yielding nonsense. We impose the asymptotic boundary at finite $\rho = \rho_{\max}$ which we typically take to be ~ 5, and thus several multiples of the half periodic compactification radius $L/2 = \pi/2$. In the next appendix we show data for varying $\rho_{\max}$ and demonstrate this has been taken large enough so as to be irrelevant.

Essentially all of our numerical problems come from the symmetry axis $r = 0$. Firstly, rather than discretising the grid in the ρ, χ coordinates, generically one gains stability using ρ, ξ with

$$\xi = 4(\chi - \pi/2)^2, \tag{A·1}$$

since at $\chi = \pi/2$, all fields are even in $(\chi - \pi/2)$ and therefore linear in ξ. This was used successfully in a black hole on an RS brane to improve stability.[19] However, even with this modification the algorithm is horribly unstable, and even for the smallest black holes we find no convergence. The same problem was encountered in the earliest application of this method.[18] When dealing with a spherically symmetric scalar field ϕ in polar coordinates, one is very familiar with terms such as $\frac{1}{r}\partial_r\phi$ in the equations of motion. Whilst for an elliptic relaxation these look as if they might destroy convergence, in reality they are not a severe problem, as long as the Neumann condition on ϕ is imposed at $r = 0$. However, the ansatz (1) or (7) generates more singular terms in the field equations. The exact form of our metric ansatz (7) guarantees that only one of the elliptic equations is affected, but we find that in the equation for C, we have

$$J\Delta C = \frac{3J}{r^2}\left(e^{-10C/3} - 1\right) + \cdots, \tag{A·2}$$

where $J\Delta = J\left(\partial_r^2 + \partial_z^2\right) = (\partial_\rho^2 + \partial_\chi^2)$. The remaining terms have the more usual $1/r$ multiplying derivatives. Obviously the above term is finite as $C \sim r^2$ near the axis. However since we do not impose the condition that C behaves quadratically near the axis, and instead it emerges from a combination of the elliptic equations and the constraints, during the early stages of the relaxation this term generically destroys convergence.

We deal with this term as in Ref. 18). The second derivative terms in the constraint equation $G^\rho{}_\chi$ are simply $C_{,\rho\chi}$ and thus have characteristics compatible with integrating C over the (ρ, χ) domain. However this equation has no singular term like that above, and any solution for C integrated away from the $r = 0$ axis has very good quadratic behaviour in r near there.[*] Thus using this constraint, we integrate for C, but call this function $C2$. Since it has very good properties near the r axis, we calculate the one singular term in the elliptic equation for C using $C2$ rather than C. Whilst this seems circular in nature, and we offer no proof why this should converge so that $C = C2$ finally, in practice this does indeed happen, and the method becomes very stable. Given the characteristics we need two initial data surfaces, one at constant χ, the other at constant ρ. For χ we fix $C2 = C$ at $\chi = \pi/2$, which includes the $r = 0$ axis for $\rho < 0$, and this ensures that the quality of the $C2$ behaviour is good near the symmetry axis. For the other initial surface we take the horizon, and fix $C2$ using the condition (13) (but now for $C2$) that the

[*] One might imagine using just $G^\rho{}_\chi$ and 2 elliptic equations for A and B, but we have been unable to find a scheme like this that works in practice, due to the non-local nature of the integration for C.

horizon temperature is a constant, giving

$$C2(\rho_0, \chi) = (B - A) - (B - A)|_{\chi=\pi/2} + \frac{1}{2}\log\left(\frac{J}{J|_{\chi=\pi/2}}\right). \tag{A·3}$$

As discussed earlier, this condition is not used when solving the elliptic equations, where we instead use the $(G^{\rho}{}_{\rho} - G^{\chi}{}_{\chi})$ constraint. However, it gives a more stable initial boundary condition for the $C2$ integration than simply setting $C2 = C$ there directly (which destroys convergence). We then integrate $C2$ from these two boundaries by quadrature:

$$C2 = \int_{\rho_0}^{\rho} d\rho \int_{\pi/2}^{\chi} d\chi\ F(\rho, \chi) + C(\rho_0, \chi) + C(\rho, \pi/2)\,. \tag{A·4}$$

Here, F is the 'source' term in the constraint equation.

The reason this method to compute the singular term in the elliptic equation for C appears to work is that in practice the contribution $(e^{-10C/3} - 1)/r^2$ is only significant near the $r = 0$ axis, and away from there this source term dies away more quickly than the other terms as it is suppressed by $1/r^2$. Thus whilst the process appears very non-local, involving integration over the lattice during the relaxation, which is not very 'gentle' and might destroy convergence, actually it only has an effect localised at the axis. Furthermore the function C is generically much smaller than the other metric functions, and therefore C appears to have relatively little effect on the solution anyway.

Since we do find stable converged solutions we may check that C is equal to $C2$, and indeed comparing these globally over our domain is an excellent check that the constraint equations are enforced. In Fig. 11 we show C and $C2$ for a black hole with $\rho_0 = -0.71$, and we see that the difference between the functions is very small compared to C, and furthermore C is very small compared to A and B. Thus, this method, whilst appearing rather mysterious, does seem to give very good results in practice.

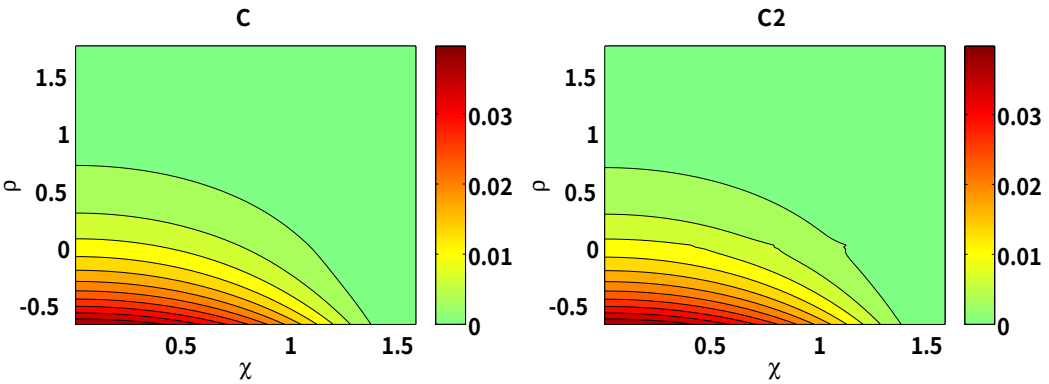

Fig. 11. Plots of the metric functions C and $C2$ for $\rho_0 = -0.71$. Main error of $C2$ originates from the coordinate singularity at $\rho = 0, \chi = \pi/2$, but its effect for C through the elliptic equation is small, and the difference of their magnitude is very small compared to C.

We reconstruct the values of A, B at the coordinate singularity $\rho = 0$, $\chi = \pi/2$ (C of course is zero), and since the ρ, χ coordinate system is singular there, it is easiest to consider this in the non-singular r, z coordinates. Then from the axial symmetry at $r = 0$ and the reflection symmetry at $z = \pi/2$, the metric functions have the expansions

$$A(r, z) = k_0 + k_1 r^2 + k_2 (\pi/2 - z)^2 + O(r^4, (\pi/2 - z)^4, r^2(\pi/2 - z)^2), \quad \text{(A·5)}$$

and similarly for B, and thus using the relation between $\{r, z\}$ and $\{\rho, \chi\}$, we may simply compute how to interpolate the values at the coordinate singularity $r = 0, z = \pi/2$ from the neighbouring points in the ρ, χ grid.

Appendix B
—— *Numerical Checks* ——

We find second order scaling in all physical quantities such as the mass, temperature and entropy. However, the resolutions are sufficiently high that increases yield very little change in the quantities. Observe the earlier Fig. 9 where we plotted the thermodynamic quantities for 3 different resolutions, which give extremely similar results where multiple resolutions may be relaxed. This gives much confidence that the accuracy of these solutions is high. Certainly our main conclusion is seen in this figure, that the black holes become larger in mass and entropy than the most non-uniform strings, and we see this is totally unaffected by changes in resolution.

As discussed in the main text, it is essential to explicitly test that the constraint equations are well satisfied, as these are not imposed directly, but only via boundary conditions and the CR relations. For $\rho_0 = -0.71$ we plot in Fig. 12 the weighted constraints Ψ and Φ. We see that they are suitably small, rising to their maximum near the symmetry axis or the coordinate singularity. However, it is very difficult to interpret these constraint violation values in terms of their physical effect. A nice check that these small violations are sufficiently small that the physics of the solution is unaffected by them is given in Table I where we show the average values of the weighted constraints and $C2 - C$ (which also gives a measure of how well $G^{\rho}{}_{\chi}$ is satisfied) over ρ and χ for three resolutions with different ρ_0. As the numerical resolution is increased, the averaged constraint violation values decrease significantly (not quite as quickly as second-order scaling, but then our discretisation geometry is rather complicated, so this would not be expected), indicating that the constraints become increasingly well satisfied, as we would hope. The geometry and other properties of the solutions vary very little as the resolution is increased, and thus the constraint violations must be very small in terms of their physical effect.

In order to assess the absolute physical error in these small constraint violations globally, we advocate comparing the values of C and $C2$ shown in the previous appendix over the whole domain. Since these agree extremely well, this is again excellent evidence that $G^{\rho}{}_{\chi}$ is effectively very well satisfied, since $C2$ is integrated from this constraint, and C is obviously derived from the elliptic equations. Yet another physical test we may perform is to compute the horizon temperature as a function of χ along the horizon. Again, the $G^{\rho}{}_{\chi}$ constraint should ensure this is

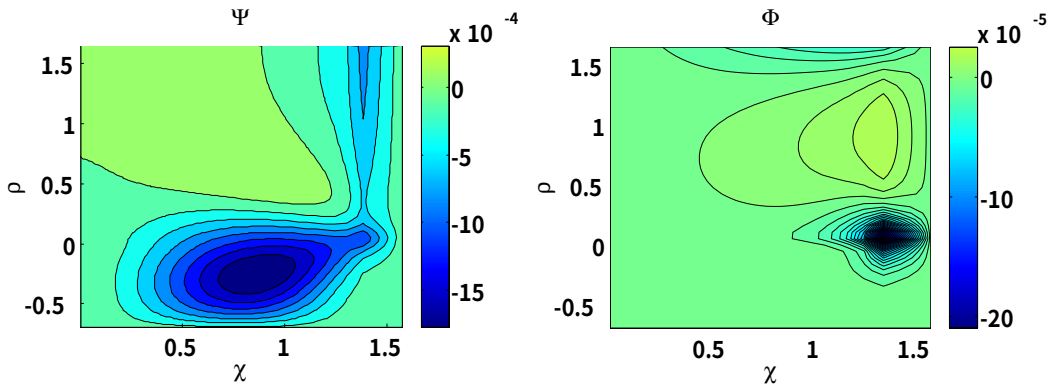

Fig. 12. Plots of the weighted constraint equations for $\rho_0 = -0.71$.

constant, yet it is the $(G^{\rho}{}_{\rho} - G^{\chi}{}_{\chi})$ constraint that we actually impose at the horizon for the elliptic equations. Thus if $G^{\rho}{}_{\chi}$ is well satisfied, then the CR constraint structure is working well. In Fig. 13 we plot the maximum variation, $\delta\mathcal{T}_{\text{error}} = (\mathcal{T}_{\max} - \mathcal{T}_{\min})/\mathcal{T}$, of the temperature with respect to variation in ρ_0 for our highest resolution, and two lower resolutions. These variations are small, implying the constraints are indeed well satisfied. Furthermore they decrease very nicely with increasing resolution indicating that the constraints behave well numerically, and are free from systematic violations. We find maximum variation for the largest black holes, as expected as gradients build up near the horizon at $\chi = \pi/2$ due to the limited resolution at the axis. However the variation is still only $\sim 1\%$ for the largest black hole we relaxed.

In Table II we show the temperature, entropy and mass for a black hole using different $\rho_{\max}$. We see these quantities (and indeed all others) hardly change, indicating that our choice of $\rho_{\max}$ is sufficiently large.

Table I. This table shows averaged violations of the weighted constraint equations and $C2 - C$ for three resolutions and three different black holes. The average of the absolute values is taken over the whole domain.

	$\langle\lvert\Psi\rvert\rangle$	$\langle\lvert\Phi\rvert\rangle$	$\langle\lvert C2 - C\rvert\rangle$
$\rho_0 = -1.1$			
140×420	4.3×10^{-5}	2.9×10^{-6}	1.0×10^{-5}
70×210	6.6×10^{-5}	7.2×10^{-6}	3.1×10^{-5}
35×105	1.5×10^{-4}	1.8×10^{-5}	8.6×10^{-5}
$\rho_0 = -0.71$			
140×420	1.8×10^{-4}	1.6×10^{-5}	3.6×10^{-5}
70×210	2.6×10^{-4}	3.2×10^{-5}	8.6×10^{-5}
35×105	5.1×10^{-4}	5.2×10^{-5}	1.7×10^{-4}
$\rho_0 = -0.36$			
140×420	7.1×10^{-4}	1.0×10^{-4}	2.2×10^{-4}
70×210	1.2×10^{-3}	2.1×10^{-4}	4.3×10^{-4}
35×105	—	—	—

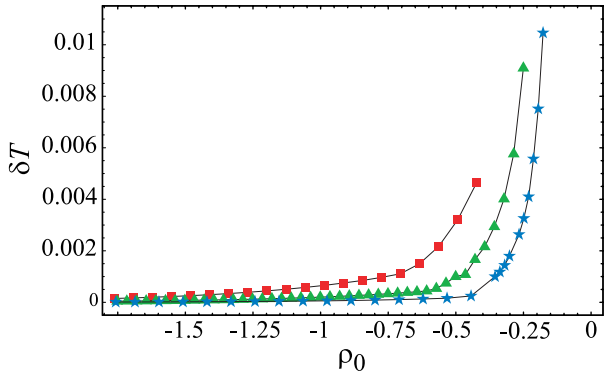

Fig. 13. Plot showing the variation of the temperature on the horizon, $\delta\mathcal{T}_{\rm error} = (\mathcal{T}_{\rm max} - \mathcal{T}_{\rm min})/\mathcal{T}$, for three resolutions: our maximum 140×420 (star), and two lower resolutions, 70×210 (triangle) and 36 × 106 (square).

Table II. This table shows the variations of the temperature, entropy and asymptotic mass for a black hole with $\rho_0 = -0.36$ using different $\rho_{\rm max}$. The variation of the quantities is defined as $\delta\mathcal{T}/\mathcal{T} = 1 - \mathcal{T}/\mathcal{T}_{\rho_{\rm max}=5.7}$, dividing by $\mathcal{T}$ for $\rho_{\rm max} = 5.7$.

70×210	$\lvert\delta\mathcal{T}/\mathcal{T}\rvert$	$\lvert\delta\mathcal{S}/\mathcal{S}\rvert$	$\lvert\delta M/M\rvert$
$\rho_{\rm max} = 4.6$	3.5×10^{-4}	1.3×10^{-3}	1.1×10^{-2}
2.5	3.6×10^{-3}	1.9×10^{-2}	9.3×10^{-2}
1.4	5.1×10^{-2}	1.8×10^{-1}	4.0×10^{-1}

Appendix C

—— Demonstration That First Law Does Not Test the Constraints ——

In this brief appendix we demonstrate our claim that deriving the asymptotic mass by integrating the First Law $dM = \mathcal{T}d\mathcal{S}$ along our branch of numerical solutions (for fixed asymptotic radius) does not test whether the constraint equations are satisfied. This is also true for the related Smarr law. Thus while it is useful to check that the First Law is satisfied, as it checks the elliptic equations are well satisfied and have boundary conditions imposed compatibly with their regular singular behaviour, we should not be lulled into a false sense of security. We satisfy the elliptic equations directly in this relaxation method, and to high accuracy, whereas the constraint equations are imposed indirectly, via the boundary conditions. Hence these are the equations we should worry may have numerical errors, and it is crucial to separately check these, as was done in the previous appendix.

The First Law can be classically derived, e.g. as in Ref. 56). Here we simply sketch the derivation, considering which components of the Einstein tensor are involved, and therefore which can be numerically tested by the First Law. Consider the expression

$$\tilde{S}(g_{\mu\nu}) = \int_{\mathcal{M}} d^6x\sqrt{-g}R(g_{\mu\nu}) \tag{C·1}$$

for a manifold $\mathcal{M}$ with metric $g_{\mu\nu}$. This is not the action, since for the action we must subtract the Gibbons-Hawking term at the boundaries $\delta\mathcal{M}$. Clearly $\tilde{S}$ (unlike

the true action) vanishes for any solution of the equations of motion, as the Ricci scalar will always vanish locally.

The First Law can be derived in our static case by considering $g_{\mu\nu} = g^{(0)}_{\mu\nu} + \delta g_{\mu\nu}$, where $g^{(0)}_{\mu\nu}$ is a static solution of the Einstein equations, *and* the perturbation $\delta g_{\mu\nu}$ also satisfies the static linearised perturbation equations. Thus, $\tilde{S}$ vanishes when evaluated on both $g^{(0)}$ and g. However, in the usual way we can write,

$$\tilde{S}(g_{\alpha\beta}) - \tilde{S}(g^{(0)}_{\alpha\beta}) = \int_{\mathcal{M}} d^6x \sqrt{-g^{(0)}} G_{\mu\nu}(g^{(0)}_{\alpha\beta}) \delta g^{\mu\nu} + [V_{\mu\nu}\delta g^{\mu\nu} + W_{\mu\nu}\partial_n \delta g^{\mu\nu}]_{\delta\mathcal{M}} + O(\delta g^2), \tag{C·2}$$

where ∂_n is the derivative normal to the boundary, and V, W give boundary terms that arise to eliminate derivatives of δg in the integral term. Since the first 3 terms all vanish, we are left simply with the boundary terms, and these give rise to the First Law, linearised in δg, when evaluated on the horizon and asymptotically. However, let us now consider the above in our numerical context. If numerically we see that the First Law is well satisfied, does this imply all the Einstein equations, both elliptic and constraints, are therefore well satisfied?

Naively it appears that indeed they are. From the terms $\tilde{S}(g_{\mu\nu})$ and $\tilde{S}(g^{(0)}_{\mu\nu})$ we test the weighted average of the Ricci scalars, $R(g)$ and $R(g^{(0)})$, and from the linear variation term we test a weighted average of $G_{\mu\nu}(g^{(0)})$. However, given that our metric (1) is diagonal, and furthermore, our perturbation δg is therefore also diagonal, these three terms then *only* test the diagonal components of the Einstein tensor. Thus these weighted integrals simply do not involve the $G^r{}_z$ Einstein equation (or equivalently $G^\rho{}_\chi$). Even worse, due to the conformal invariance of the r, z (or equivalently f, g) block of the metric, the perturbation is restricted such that $\delta g_{rr} = \delta g_{zz}$, and therefore the integrals also do not involve $(G^r{}_r - G^z{}_z)$ (or equivalently $(G^\rho{}_\rho - G^\chi{}_\chi)$).

Now it is clear that if we take any solution of the elliptic equations, $\tilde{g}^{(0)}$, completely ignoring the constraints, and perturb this by $\delta\tilde{g}$ which again only satisfies the static linearised elliptic equations, we can perform exactly the same manipulations to obtain the above equation, and consequently the usual First Law. Hence for 'solutions' obeying only the elliptic equations we would still see that the First Law being well observed, even though we made no attempt to satisfy the constraint equations.

Thus, our specific form of the metric exactly ensures that the Einstein equations that are the 'constraints' in this elliptic context, $G^r{}_z$ and $(G^r{}_r - G^z{}_z)$, do not affect the First Law, even if they are not satisfied due to numerical error. For exactly the same reasons, the closely related Smarr law also has no dependence on the constraint equations, when using our metric choice, and similarly cannot provide a numerical test of the constraints.

References

1) L. Randall and R. Sundrum, Phys. Rev. Lett. **83** (1999), 4690; hep-th/9906064.
2) T. Kaluza, Sitzungsber. Preuss. Akad. Wiss. Berlin (Math. Phys.) **K1** (1921), 966.
3) O. Klein, Z. Phys. **37** (1926), 895.
4) N. Arkani-Hamed, S. Dimopoulos and G. Dvali, Phys. Lett. B **429** (1998), 263; hep-ph/9803315.
5) I. Antoniadis, N. Arkani-Hamed, S. Dimopoulos and G. Dvali, Phys. Lett. B **436** (1998), 257; hep-ph/9804398.
6) G. Gibbons and D. Wiltshire, Ann. of Phys. **167** (1986), 201.
7) A. Chodos and S. Detweiler, Gen. Relat. Gravit. **14** (1982), 879.
8) R. Gregory and R. Laflamme, Phys. Rev. D **37** (1988), 305.
9) R. Gregory and R. Laflamme, Phys. Rev. Lett. **70** (1993), 2837; hep-th/9301052.
10) R. Gregory and R. Laflamme, Nucl. Phys. B **428** (1994), 399; hep-th/9404071.
11) S. Gubser, Class. Quantum Grav. **19** (2002), 4825; hep-th/0110193.
12) T. Wiseman, Class. Quantum Grav. **20** (2003), 1137; hep-th/0209051.
13) R. Myers, Phys. Rev. D **35** (1987), 455.
14) D. Korotkin and H. Nicolai, gr-qc/9403029.
15) A. Frolov and V. Frolov, Phys. Rev. D **67** (2003), 124025; hep-th/0302085.
16) R. Emparan and H. Reall, Phys. Rev. D **65** (2002), 084025; hep-th/0110258.
17) T. Harmark and N. Obers, J. High Energy Phys. **05** (2002), 032; hep-th/0204047.
18) T. Wiseman, Phys. Rev. D **65** (2002), 124007; hep-th/0111057.
19) H. Kudoh, T. Tanaka and T. Nakamura, Phys. Rev. D **68** (2003), 024035; gr-qc/0301089.
20) H. Kudoh, Prog. Theor. Phys. **110** (2004), 1059; hep-th/0306067.
21) T. Tanaka, Prog. Theor. Phys. Suppl. No. 148 (2003), 307; gr-qc/0203082.
22) R. Emparan, A. Fabbri and N. Kaloper, J. High Energy Phys. **08** (2002), 043; hep-th/0206155.
23) B. Kol, hep-th/0206220.
24) B. Kol, hep-ph/0207037.
25) E. Sorkin and T. Piran, Phys. Rev. Lett. **90** (2003), 171301; hep-th/0211210.
26) T. Harmark and N. Obers, hep-th/0309116.
27) B. Kol, E. Sorkin and T. Piran, hep-th/0309190.
28) T. Harmark and N. Obers, hep-th/0309230.
29) T. Wiseman, Class. Quantum Grav. **20** (2003), 1177; hep-th/0211028.
30) B. Kol and T. Wiseman, Class. Quantum Grav. **20** (2003), 3493; hep-th/0304070.
31) R. Emparan and H. Reall, Phys. Rev. Lett. **88** (2002), 101101; hep-th/0110260.
32) B. Kol, hep-th/0208056.
33) L. Randall and R. Sundrum, Phys. Rev. Lett. **83** (1999), 3370; hep-ph/9905221.
34) A. Chamblin, S. Hawking and H. Reall, Phys. Rev. D **61** (2000), 065007; hep-th/9909205.
35) R. Gregory, Class. Quantum Grav. **17** (2000), L125; hep-th/0004101.
36) G. Gibbons and S. Hartnoll, Phys. Rev. D **66** (2002), 064024; hep-th/0206202.
37) T. Tamaki, S. Kanno and J. Soda, hep-th/0307278.
38) S. Gubser and I. Mitra, hep-th/0009126.
39) S. Gubser and I. Mitra, J. High Energy Phys. **08** (2001), 018; hep-th/0011127.
40) H. Reall, Phys. Rev. D **64** (2001), 044005; hep-th/0104071.
41) J. Gregory and S. Ross, Phys. Rev. D **64** (2001), 124006; hep-th/0106220.
42) V. Hubeny and M. Rangamani, J. High Energy Phys. **05** (2002), 027; hep-th/0202189.
43) S. Gubser and A. Ozakin, J. High Energy Phys. **05** (2003), 010; hep-th/0301002.
44) G. Gibbons, S. Hartnoll and C. Pope, Phys. Rev. D **67** (2003), 084024; hep-th/0208031.
45) S. Hartnoll, hep-th/0305001.
46) R. Myers and M. Perry, Ann. of Phys. **172** (1986), 304.
47) H. Reall, Phys. Rev. D **68** (2003), 024024; hep-th/0211290.
48) R. Emparan and R. Myers, hep-th/0308056.
49) G. Horowitz, hep-th/0205069.
50) M. Choptuik et al., gr-qc/0304085.
51) E. Sorkin, B. Kol and T. Piran, hep-th/0310096.
52) B. Kleihaus and J. Kunz, Phys. Rev. D **57** (1998), 834; gr-qc/9707045.
53) M. Choptuik, E. Hirschmann, S. Liebling and F. Pretorius, Class. Quantum Grav. **20** (2003), 1857; gr-qc/0301006.

54) S. Hawking and G. Horowitz, Class. Quantum Grav. **13** (1996), 1487; gr-qc/9501014.
55) P. Townsend and M. Zamaklar, Class. Quantum Grav. **18** (2001), 5269; hep-th/0107228.
56) R. Wald, *Quantum field theory in curved space-time and black hole thermodynamics* (Chicago, USA: Univ. Pr., 1994), p. 205.